Journal of Magnetic Resonance **153,** 92–102 (2001)
doi:10.1006/jmre.2001.2434, available online at http://www.idealibrary.com on IDEAL®

Electron Spin Relaxation in Pseudo-Jahn–Teller Low-Symmetry Cu(II) Complexes in Diaqua(L-Aspartate)Zn(II) · H_2O Crystals

S. K. Hoffmann,*[,1] W. Hilczer,* J. Goslar,* M. M. Massa,† and R. Calvo‡

*Institute of Molecular Physics, Polish Academy of Sciences, Smoluchowskiego 17, PL-60179 Poznan, Poland; †Facultad de Ciencias Exactas, Ingenieria Agrimensura, Universidad Nacional de Rosario, Avda. Pellegrini 250, 2000 Rosario, Argentina; and ‡Facultad de Bioquímica y Ciencias Biológicas, Universidad Nacional del Litoral and INTEC (CONICET-UNL), Güemes 3450, 3000 Santa Fe, Argentina

Received April 25, 2001; revised August 21, 2001; published online October 5, 2001

Low-temperature (4–55 K) pulsed EPR measurements were performed with the magnetic field directed along the *z*-axis of the *g*-factor of the low-symmetry octahedral complex [^{63}Cu(L-aspartate)$_2$(H_2O)$_2$] undergoing dynamic Jahn–Teller effect in diaqua(L-aspartate)Zn(II) hydrate single crystals. Spin–lattice relaxation time T_1 and phase memory time T_M were determined by the electron spin echo (ESE) method. The relaxation rate $1/T_1$ increases strongly over 5 decades in the temperature range 4–55 K. Various processes and mechanisms of T_1-relaxation are discussed, and it is shown that the relaxation is governed mainly by Raman relaxation processes with the Debye temperature $\Theta_D = 204$ K, with a detectable contribution from disorder in the doped Cu^{2+} ions system below 12 K. An analytical approximation of the transport integral I_8 is given in temperature range $T = 0.025$–$10\ \Theta_D$ and applied for computer fitting procedures. Since the Jahn–Teller distorted configurations differ strongly in energy ($\delta_{12} = 240\ cm^{-1}$), there is no influence of the classical vibronic dynamics mechanism on T_1. Dephasing of the ESE (phase relaxation) is governed by instantaneous diffusion and spectral diffusion below 20 K with resulting rigid lattice value $1/T_M^0 = 1.88$ MHz. Above this temperature the relaxation rate $1/T_M$ increases upon heating due to two mechanisms. The first is the phonon-controlled excitation to the first excited vibronic level of energy $\Delta = 243\ cm^{-1}$, with subsequent tunneling to the neighbor potential well. This vibronic-type dynamics also produces a temperature-dependent broadening of lines in the ESEEM spectra. The second mechanism is produced by the spin–lattice relaxation. The increase in T_M is described in terms of the spin packets forming inhomogeneously broadened EPR lines. © 2001 Academic Press

Key Words: **ESE; Cu^{2+} electron spin relaxation; ESEEM; Cu^{2+} Jahn–Teller effect.**

I. INTRODUCTION

Electron spin relaxation consists of two processes. One is the fast dephasing of the precessional motion of spins (described by the spin–spin relaxation time T_2) or dephasing of the spin packets (described by the phase memory time T_M). The other is the slower process of recovery of the population of the Zeeman levels to the Boltzmann equilibrium value after excitation (described by the spin–lattice relaxation time T_1). In the majority of cases T_2 is too short to be measured by pulsed EPR techniques. $T_1 \gg T_M$ at low temperatures, and both T_1 and T_M can be measured by the electron spin echo (ESE) method.

Spin–lattice relaxation processes and mechanisms seem to be better understood than those producing dephasing, but nonresolved theoretical and experimental problems still exist. Spin–lattice relaxation theories suffer from crude approximations of the spin–phonon coupling coefficient (*1–3*), whereas the experimental problem is how to differentiate various contributions to T_1 (*4, 5*) and even how to avoid artifacts in the determination of T_1 from the relaxation curves (*3, 6*). Since the T_1-magnitude is not well reproduced by existing theories, the main source of information is its temperature dependence. For paramagnetic ions diluted in ionic dielectric crystals the relaxation rate $1/T_1$ increases several orders of magnitude upon heating from liquid helium temperature to room temperature and is governed mainly by two-phonon Raman processes. In such a case, theoretical calculations of the relaxation rate assume the Debye model of lattice vibrations with a density of phonon states $\rho(\omega) \propto \omega^2$, although it is well known that this model is far from the real phonon spectra of even simple crystals. Some modifications have been proposed with $\rho(\omega) \propto \omega^p$ ($p < 2$) (*7, 8*) or by making the Debye cutoff frequency less abrupt (*9*). For a description of the temperature dependence of $1/T_1$ for the Raman processes the transport integrals over a Debye phonon spectrum must be calculated numerically (*10*). Recently we proposed an analytical approximation of the I_8 transport integral for Kramers transitions, appropriate for Cu^{2+} ions, and valid for the temperature range $T = 0.055$–$2.5\ \Theta_D$ (*11*), where Θ_D is the Debye temperature. In this paper a better approximation, which can be easily used in computer fitting procedures, is proposed and extended to the lower temparature range, valid for $T = 0.025$–$10\ \Theta_D$.

Additional complications arise in Jahn–Teller active paramagnetic centers where local vibronic dynamics influences directly or indirectly the spin–lattice relaxation via various mechanisms of the potential barrier crossing (*12, 13*). In disordered,

[1] To whom correspondence should be addressed. Fax (0-48) 61 8684 524.

1090-7807/01 $35.00

amorphous, or polymeric systems the concept of phonons has restricted validity, and the relaxation rate is weakly affected by temperature and governed by local molecular dynamics (*14*). The relaxation of free radicals produced by ionizing radiation in molecular crystals can also be governed by local disorder and molecular dynamics (*15, 16*), indicating that ordinary phonon relaxation processes are not active.

Various spin–lattice relaxation processes and mechanisms are shortly reviewed in this paper and applied to the analysis of experimental data for low symmetry octahedral Cu^{2+} complexes undergoing the pseudo-Jahn–Teller effect. We also identify the influence of the nonuniform Cu^{2+}distribution on the relaxation rate at low temperatures.

The electron spin relaxation times were determined using the electron spin echo technique. The ESE signal can be generated and ESE dephasing time T_M can be measured for inhomogeneously broadened EPR lines only. The existing theories of the ESE dephasing (phase relaxation) describe various mechanisms producing random changes in the precession phase (*17–19*). These theories were verified for simple model systems where the decay of the ESE amplitude after excitation was weakly or not disturbed by the Larmor precession of the surrounding magnetic nuclei. In most cases, however, the decay is complicated by the strong modulations produced by a weak dipolar coupling between unpaired electrons and the nuclei. The problems are how to separate the decay and modulation functions and how to differentiate various types of theoretically predicted exponential decays. For paramagnetic center concentration higher than 10^{18} spin/cm^3 the phase relaxation is governed by the spectral and instantaneous diffusion within the unpaired electron system. For lower concentration the effects from the nuclear spectral diffusion and the temperature-dependent dephasing mechanisms can have dominant contributions. In this paper we identify the contributions of the vibronic dynamics and spin–lattice relaxation to the temperature dependence of the dephasing rate $1/T_M$. The vibronic dynamics effects are not detectable in the spin–lattice relaxation of Cu^{2+} in Zn(L-aspartate) · $3H_2O$ because of the relatively slow reorientations between strongly nonequivalent Jahn–Teller distorted configurations. In contrast to this, the phase relaxation is sensitive to these reorientations because of very narrow spin packets forming EPR lines. It allows one to determine the energy of excited vibronic levels from temperature variations of $1/T_M$. This is a very unique property of ESE phase relaxation, and we will show that the vibronic dynamics also influences the linewidth of the ESEEM spectrum lines. This ENDOR-type spectrum is obtained from the Fourier transform of the ESE modulation function.

Contribution from spin–lattice relaxation processes is generally underestimated in published papers, but we have shown previously (*5, 20*) and we will show here that this mechanism contributes to the dephasing rate at intermediate and high temperatures.

Aspartic acid $COOHCH_2CHNH_2COOH$ salts are interesting as model systems to study metal–protein interactions (*21*).

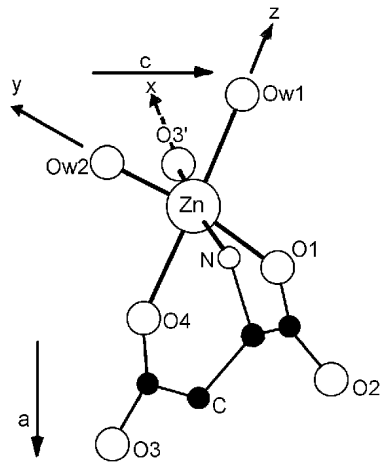

FIG. 1. Projection of the structure of Zn(L-aspartate) · $3H_2O$ onto the *ac*-plane. The local *x, y, z* axes of the EPR *g*-tensor are marked. Cu^{2+} ions substitute the Zn^{2+} ions, and the *z* and *y* directions are Jahn–Teller active.

Copper(II) complexes with aspartic acid were studied in solution and in solids and characterized by structural (*22*), spectroscopic (*22*), and magnetic (*22, 23*) methods. The aspartate molecule is potentially a tridentate ligand (*21*) and the metal complexes in Cu(L-aspartate) · $2H_2O$ (*22*) and in Zn(L-aspartate) · $3H_2O$ (*24*) have different structures. The Cu^{2+} ion in the copper salt is five-coordinated in a distorted tetragonal pyramidal coordination. It has two water molecules, the terminal carboxylate oxygen of one aspartate molecule, the residual carboxylate oxygen, and a nitrogen atom of the adjacent aspartate molecule as its nearest ligands. In the zinc compound, the Zn^{2+} ions are in a distorted octahedral coordination with aspartate ions as tridentate ligands and bonded to two water molecules and an oxygen of an other aspartate ion (Fig. 1). Recent EPR studies (*24*) have shown that Cu^{2+} ions doped into Zn(L-aspartate) · $3H_2O$ crystals display a vibronic-type behavior with *g*-factors and hyperfine splittings averaged gradually on heating. In the temperature range 100–300 K, this behavior was described in terms of the pseudo-Jahn–Teller effect, assuming Boltzmann equilibrium between two Jahn–Teller configurations of the octahedron distorted along the O–Cu–H_2O bonds (*24*). In this simple model (*25, 26*) the minima in the adiabatic potential surface are strongly nonequivalent with an energy difference $\delta_{12} = 240\ cm^{-1}$. The third minimum, located at about 440 cm^{-1}, corresponds to a configuration elongated along the O–Cu–N bond. This state is practically unpopulated below room temperature. A two-well model has been used to describe the vibronic dynamics of octahedral $Cu(H_2O)_6^{2+}$ complexes in Tutton salt crystals (*25–27*). In Zn(L-aspartate) · $3H_2O$:Cu^{2+} this model is valid above 100 K, when the two lowest energy distorted configurations are thermally populated. Below this temperature the Cu^{2+} complexes undergo relatively slow reorientations between these two configurations. This slow reorientations produce, however, the well-measured effects in the electron spin phase relaxation.

II. EXPERIMENTAL

Zn(L-aspartate) · $3H_2O$ was obtained from a hot water solution (100° C) of stoichiometric quantities of L-aspartic acid and zinc carbonate hydroxide. Large rod-shaped single crystals were grown from saturated solution at 60°C. They belong to the space group $P2_12_12_1$ ($Z = 4$) (*24*), are elongated along the [010] direction, and have well-developed {110} faces. The crystals were doped with a 0.1% Cu/Zn ratio by adding copper(II) nitrate trihydrate enriched with 99% ^{63}Cu to the mother solution. The concentration of copper ions in the crystal was evaluated by EPR to be 7×10^{18} spin/cm^3.

Pulsed EPR experiments were performed using a Bruker ESP380E FT/CW spectrometer equipped with an Oxford CF935 flow helium cryostat. Electron spin relaxation times were determined from measurements of a single crystal with the magnetic field along the molecular *z*-axis (*g*-tensor *z*-axis) of one of the four magnetically nonequivalent Cu^{2+} sites in the crystal unit cell (see Fig. 1). The EPR spectrum recorded by the field-swept electron spin echo method along this direction at 10 K is shown in Fig. 2. This absorption-type EPR spectrum consists of four hyperfine quartets (I–IV) from the four nonequivalent Cu^{2+} sites. The lines corresponding to sites III and IV are split into 1 : 1 : 1 triplets due to the hyperfine interaction with the ^{14}N nucleus of the aspartate ligand. In the pulsed EPR experiments reported here the low-field hyperfine line of site I (marked by arrow in Fig. 2) was excited by microwave pulses. Thus, only 1/16 of the total amount of Cu^{2+} ions were excited. The experiments were performed in the temperature range 4–55 K, since the electron spin echo signal was nondetectable at higher temperatures.

The electron spin–lattice relaxation time T_1 was determined by the saturation recovery method. The full saturation, recognized by the vanishing of the ESE signal, was achieved with a 24-ns pulse (41.7 MHz = 14.9 G spectral width). The magnetization recovery was single exponential (see inset in Fig. 3) in the whole temperature range and was monitored with a two- pulse Hahn ESE signal generated by two 16-ns pulses separated by a 148-ns time interval.

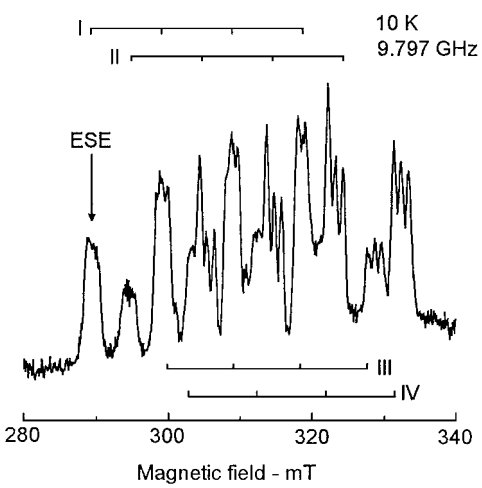

FIG. 2. Field-swept ESE spectrum along the g_z-axis at 10 K. I–IV indicate the hyperfine quartets of the four magnetically nonequivalent copper(II) sites in the unit cell. The arrow marks the line for which the pulsed EPR experiments were performed.

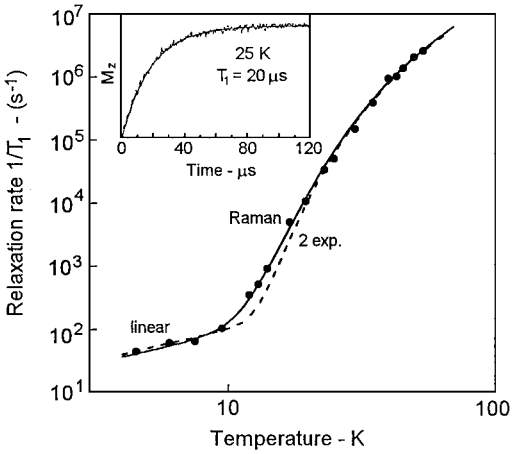

FIG. 3. Log-log plot of the temperature dependence of the spin–lattice relaxation rate measured with magnetic field $B \| g_z$. The solid line is the best fit assuming linear and two-phonon Raman relaxation processes (Eq. [5]) as described in the text. The dashed line is the best fit with Eq. [6] describing the Orbach–Aminov-type relaxation processes via two excited vibronic states. The inset shows the recovery of magnetization at 25 K.

The phase memory time T_M, describing the phase relaxation of the precessing spin packets, was determined from the decay of the ESE amplitude using two 16-ns pulses for the ESE generation. The decay was strongly modulated by the weak dipolar coupling with surrounding magnetic nuclei. Thus, the observed ESE amplitude decay was described by $V(2\tau) = V_{\text{decay}} \cdot V_{\text{mod}}$, where τ is the interpulse interval. To single out these two contributions is not trivial and is based on computer simulations using existing theories of phase relaxation.

We have found weak effects from instantaneous diffusion indicating that the concentration of the Cu^{2+} ions is not low enough to avoid dipolar Cu–Cu interactions.

III. ELECTRON SPIN–LATTICE RELAXATION

1. Theoretical Temperature Dependence of the Relaxation Rate in Solids

The primary mechanism of the spin–lattice relaxation of noninteracting paramagnetic centers is a phonon modulation of the electric crystal field that influences the spin orientation via the spin–orbit coupling. This mechanism can act via various acoustic phonon processes usually involving the direct one-phonon process, two-phonon Raman processes, or excitations to high-energy orbital levels (Orbach–Aminov process). They are described in Krönig–Van Vleck theory (*1–3*), which for Cu^{2+}

(Kramers ion) gives

$$\frac{1}{T_1} = A_{\mathrm{dir}}T + A_{\mathrm{Ram}}T^9 I_8\left(\frac{\Theta_{\mathrm{D}}}{T}\right) + A_{\mathrm{Orbach}}\Delta^3 \exp\left(-\frac{\Delta_{\mathrm{orb}}}{kT}\right). \quad [1]$$

The linear term dominates below the liquid helium temperature. The Raman term (T^9 temperature dependence modified by the transport integral $I_8(\Theta_{\mathrm{D}}/T)$ taken over the Debye-type phonon spectrum up to the Debye temperature Θ_{D}) dominates at higher temperatures in ionic and molecular crystals. The exponential term is the contribution of the Orbach–Aminov process, produced via an orbital level of energy Δ_{orb}. The A-coefficients in Eq. [1] depend on details of the electron–phonon coupling.

Besides the above-described classical spin–lattice relaxation processes, one may consider the following contributions to $1/T_1$:

$$\frac{1}{T_1} = A_{\mathrm{loc}}\,\mathrm{cosech}\left(\frac{\Delta_{\mathrm{l}}}{kT}\right) + A_{\mathrm{opt}}\,\mathrm{cosech}^2\left(\frac{\Delta_{\mathrm{ph}}}{2kT}\right) + A_{\mathrm{bottl}}T^2 + A_{\mathrm{therm}}\left(\frac{2\tau_{\mathrm{c}}}{1+\omega^2\tau_{\mathrm{c}}^2}\right). \quad [2]$$

The term $\mathrm{cosech}(x) = 2/(e^x - e^{-x})$, with $(x = \Delta_{\mathrm{l}}/kT)$, describes the contribution from a local vibration mode (Murphy's mechanism) and can be understood as a phonon absorption with excitation of a local vibration and electron spin flip. It is described in terms of a double-well oscillator with Δ_{l} being the tunneling splitting that determines the tunneling frequency between the two wells (*28*). This term is practically linear $(1/T_1 \propto T)$ for $kT > \Delta_{\mathrm{l}}$. Some authors (*29*) use the expression $[e^x/(e^x-1)^2]$ instead of $\mathrm{cosech}(x)$ in Eq. [2] as a low-temperature approximation. Murphy's mechanism (*28*) often dominates in organic materials where it is related to a local vibration mode, methyl group tunneling rotation, or torsional oscillations of molecular groups (*15*).

Most relaxation mechanisms assume that the long-wave acoustic phonons play a dominant role in modulating the crystal field. However, at high temperatures the optical phonons, having high density of states, can give an important contribution to $1/T_1$. A contribution from optical phonons can be expected also in organic crystals, where often the optical mode energy can be the same magnitude as the Debye energy. The term proportional to $\mathrm{cosech}^2(x)$ in Eq. [2] describes the relaxation through an optical phonon of energy Δ_{ph} (*30*). The quadratic term in Eq. [2] describes the *bottleneck* effect resulting from the overheating of the phonon mode at low temperatures (*31*). The last term considers the contribution from any dynamical process produced by random molecular and spin dynamics, having exponential correlation function characterized by the correlation time τ_{c} of the process. In particular, this process can be thermally activated with τ_{c} given by the Arrhenius equation $\tau_{\mathrm{c}} = \tau_0 \exp(E_{\mathrm{a}}/RT)$. This term is analogous to the dipolar nuclear spin–lattice relaxation in NMR and describes also the electron spin cross-relaxation via dipolar coupling between two different types of paramagnetic centers (*32*).

In disordered, amorphous, or glassy solids, or in biological materials, the concept of phonons is limited, and the spin–lattice relaxation is governed mainly by modulation of the hyperfine coupling by tunneling two-level systems (TLS), by a cross-relaxation between isolated ions and exchange-coupled pairs having singlet–triplet gap Δ_{ST}, or by exchange coupling between the pairs of ions. These mechanisms lead to a temperature dependence described by the equation

$$\frac{1}{T_1} = A_{\mathrm{TLS}}\frac{1}{\omega^2}\int_{x_{\min}}^{x_{\max}} \frac{x}{\sinh x}\,dx + A_{\mathrm{cross}}\Delta_{\mathrm{ST}}\,\mathrm{cosech}\left(\frac{\Delta_{\mathrm{ST}}}{kT}\right) + A_{\mathrm{pair}}\left[\exp\left(\frac{\Delta_{\mathrm{ST}}}{kT}+1\right)\right]^{-1}. \quad [3]$$

The first term describes relaxation of a spin coupled to the nearby TLS with the integration over the TLS energy distribution from $x_{\min} = E_{\min}/kT$ to $x_{\max} = E_{\max}/kT$ (*14, 33–35*). The second term describes the cross-relaxation between single ions and exchange coupled pairs (*14, 36*) (see A_{loc} in Eq. [2] for a comparison) and the last term describes the relaxation of the pairs (*9, 14, 37*). Since $1/\sin\mathrm{h}(x) = \mathrm{cosech}(x)$ the first two contributions exhibit similar temperature dependence but for the TLS mechanism the frequency dependence is characteristic. In limiting cases of low and high temperatures both contributions can be approximated by the aT^2 and bT terms, respectively. Thus, at low temperatures (below about 8 K) the relaxation rate exhibits T^2 dependence, which changes to linear temperature dependence as the temperature increases and to an exponential-type relaxation at higher temperatures (above 40 K). A similar temperature behavior is expected in doped or irradiated crystals with strongly inhomogeneous distribution of paramagnetic centers or when the doping level is larger than 1% (*9, 15*).

For Jahn–Teller active paramagnetic centers, like Cu^{2+} complexes, the reorientations between Jahn–Teller distorted configurations (interconversions of the elongation axis between the three directions in octahedral coordination) give rise to a mechanism of spin–lattice relaxation. The reorientations can modulate anisotropic spin interactions, like g-factor and/or hyperfine anisotropy, producing spin flips. In such a case the spin–lattice relaxation time is much longer (about two orders of magnitude for Cu^{2+} ions) than the correlation time τ_{r} of the reorientations and, moreover, a strong angular variation of T_1 is predicted with temperature dependence (*13, 38*),

$$\frac{1}{T_1} = A_{\mathrm{JT}}T + B_{\mathrm{JT}}T^3 I_2\left(\frac{\Theta_{\mathrm{D}}}{T}\right) + C_{\mathrm{JT}}T^5 I_4\left(\frac{\Theta_{\mathrm{D}}}{T}\right) + D_{\mathrm{JT}}\exp\left(-\frac{\Delta_{\mathrm{vibronic}}}{kT}\right), \quad [4]$$

where the coefficients A–D depend on the reorientation time

τ_r. The meanings of the terms in Eq. [4] are as follows. At low temperatures, in the static Jahn–Teller limit, the reorientations can appear via tunneling between the ground states when the potential wells are equivalent. This mechanism is described by linear and T^3 terms in Eq. [4] with A_{JT} and B_{JT} dependent on $|3\Gamma|^2$, where 3Γ is the tunneling splitting of the ground vibronic state. At higher temperatures the dynamic Jahn–Teller effect becomes effective with reorientations produced by two mechanisms (*12*): (a) phonon-assisted tunneling via a virtual phonon state of energy δ_{12}, the energy difference between two potential wells. This mechanism leads to the linear and T^5 terms in Eq. [4] with A_{JT} and C_{JT} coefficients depending on δ_{12}; (b) phonon-controlled tunneling via an excited vibronic state of energy $\Delta_{vibronic}$. This mechanism is described by the exponential term in the Eq. [4]. The exponential term describes simultaneously the Orbach–Aminov-type relaxation processes via an excited vibronic state of energy $\Delta_{vibronic}$. Such a process is allowed due to mixing of the electronic and nuclear wavefunctions in the vibronic state and is not allowed for pure vibrational levels. The phonon-controlled and the Orbach–Aminov processes produce similar temperature dependence of $1/T_1$ but differ in the D_{JT} coefficient value. For the first process the D_{JT} is of the order of the tunneling frequency (10^6–10^7 s^{-1}), whereas for the second process D_{JT} is of the order of the vibronic frequency (10^{12}–10^{13} s^{-1}).

The vibronic energy $\Delta_{vibronic}$ is about 100–300 cm^{-1}, and we found that such exponential type of spin–lattice relaxation dominates for Cu^{2+} in SrF_2 crystals (*39*).

Beside the modulation mechanisms described above, there also exists also a direct coupling via phonons between states of opposite spin in different Jahn–Teller distorted configurations, as a consequence of the spin–orbit coupling. In this mechanism the reorientation rate $1/\tau_r$ and the relaxation rate $1/T_1$ are identical, and in the case of the spin–orbit phonon-induced tunneling process the relaxation is described by the linear and T^5 terms in Eq. [4] but with A_{JT} and C_{JT} coefficients depending on the spin–orbit coupling constant $|\lambda|^2$, as was found for paramagnetic centers in diamond (*40*). The relationship between T_1 and the reorientation rate was studied theoretically also for spin–orbit tunneling phonon-controlled processes in the case of strong nonequivalence of the potential wells (*41*). A characteristic feature of the spin–orbit-driven mechanisms is the independence of the direct relaxation process (linear term) on the magnetic field and the very broad temperature range where this linear term can dominate (*42*).

2. Experimental Temperature Variations of T_1

Equations [1–4] indicate that identification of the relaxation mechanism from the observed temperature variation of T_1 can not be unique. Figure 3 shows that the dependence of $1/T_1$ with T for Zn(L-aspartate) $\cdot$ $3H_2O$:Cu^{2+} is monotonic in the whole temperature range. Thus, the large number of possible processes and mechanisms does not allow unique fitting of the experimental data by the equations, and any fit must be supported by physical arguments or other pieces of information.

Cw-EPR data on Zn(L-aspartate) $\cdot$ $3H_2O$:Cu^{2+} (*24*) have proved that the dynamical pseudo-Jahn–Teller effect operates in the low-symmetry octahedral [Cu(L-aspartate)$_2$(H_2O)$_2$] complexes. Thus, we have analyzed whether our experimental data can be fit with Eq. [4]. The results were very unsatisfactory and the observed increase of $1/T_1$ from 5×10^1 s^{-1} to 4×10^6 s^{-1} in the temperature range 4–55 K was too large to be described considering only the reorientation mechanism. This is not surprising because the vibronic dynamics of Cu^{2+} is rather slow in this temperature range, as indicated by a relatively small onset of the vibronic averaging of the g-factors at low temperatures (Fig. 8 of Ref. (*24*)). Moreover, the energy difference $\delta_{12} = 240$ cm^{-1} between the two lowest Jahn–Teller distorted configurations is large. At temperatures below 55 K, where the relaxation measurements were performed, all Cu^{2+} complexes are practically localized in the deepest potential well, i.e., are elongated along the H_2O–Cu–O_4 direction (see Fig. 1).

Since the EPR spectra do not show any disorder in the crystal and the magnetization recovery after pulse excitation is single exponential in the whole temperature range (see inset in Fig. 3), there is no reason to expect relaxation via TLS-type systems. There are no EPR-detectable strongly coupled Cu–Cu pairs in the studied crystal. However, a weakly coupled pair may exist, as suggested by the instantaneous diffusion effects. Such pairs will produce the aT-type temperature dependence above 8 K (see the discussion of Eq. [3]). Beside the reorientation of H_2O molecules, there are no other local oscillators in the Zn(L-aspartate) $\cdot$ $3H_2O$ crystal, and the only thermally activated processes are the Jahn–Teller reorientations. Moreover, an effect from optical phonons is not expected at low temperatures and the low-temperature bottleneck effect (T^2-dependence) is not observed. Thus, we can assume that our experimental data can be described by Krönig-Van Vleck theory (Eq. [1]) with a contribution from exchange coupled pairs and with possible multiexponential contributions from the D_{JT} terms of Eq. [4] since the single exponential function does not fit the temperature data.

In order to be able to fit the data with Eq. [1] we obtained an analytical approximation of the transport integral $I_8(\frac{\Theta_D}{T}) = \int_0^{\Theta_D/T} \frac{e^z z^8}{(e^z-1)^2}\, dz$ for $\Theta_D/T = 0.1$–40.0 using numerical data given in Ref. (*10*). This integral can be approximated by a polynomial function of $\ln(\Theta_D/T)$ for $\Theta_D/T = 0.1$–15.0 and by an exponential function for $\Theta_D/T = 15.0$–40.0 as shown in Table 1.

The best fit of the data was obtained considering the linear and Raman terms:

$$\frac{1}{T_1} = aT + A_{Ram} T^9 I_8\left(\frac{\Theta_D}{T}\right). \qquad [5]$$

The fit gives $a = 9$ K^{-1} s^{-1}, $A_{Ram} = 1.0 \times 10^{-12}$ K^{-9} s^{-1}, and $\Theta_D = 204$ K and is shown by the solid line in Fig. 3. The a and

TABLE I
Analytical Approximation of the Transport Integral $I_8(x) = \int_0^x \frac{e^z z^8}{(e^z-1)^2}\,dz$ with $x = \Theta_D/T$ in the range x = 0.1–40.0

Range: $x = 0.1$–15.0

$$I_8 = \exp\{A_0 + A_1 \ln x + A_2(\ln x)^2 + A_3(\ln x)^3 + \cdots + A_9(\ln x)^9\}$$

$A_0 = -2.00976,\ A_1 = 6.87231,\ A_2 = -0.12936,\ A_3 = -0.0788,\ A_4 = -0.03222,$
$A_5 = -0.01593,\ A_6 = -0.00549,\ A_7 = 9.85532 \cdot 10^{-4},\ A_8 = 6.21152 \cdot 10^{-4},\ A_9 = -1.857 \cdot 10^{-5}$

Range: $x = 15.0$–40.0

$$I_8 = y_0 + a_1 \exp[-(x - x_0)/t_1]$$

$Y_0 = 40486.52036,\ x_0 = 15,\ a_1 = -1534.32091,\ t_1 = 1.79496$

A_{Ram} values are typical for Cu^{2+} complexes. The relatively good fit was obtained also with two exponential functions (dashed line in Fig. 3),

$$\frac{1}{T_1} = aT + D_1 \exp\left(-\frac{\Delta_1}{kT}\right) + D_2 \exp\left(-\frac{\Delta_2}{kT}\right), \qquad [6]$$

with $a = 10\ \mathrm{K}^{-1}\ \mathrm{s}^{-1}$, $D_1 = 7 \times 10^7\ \mathrm{s}^{-1}$, $D_2 = 15 \times 10^7\ \mathrm{s}^{-1}$, and vibronic level energies $\Delta_1 = 117\ \mathrm{cm}^{-1} = 168$ K and $\Delta_2 = 236\ \mathrm{cm}^{-1} = 340$ K. The value of the coefficients D_i suggests phonon-controlled tunneling between potential wells.

The Raman process gives a reasonable value of the Debye temperature $\Theta_{\mathrm{D}} = 204$ K. The relaxation via the excited vibronic levels gives reasonable Δ-values, with the ratio $\Delta_2/\Delta_1 \approx 2$ expected from a harmonic oscillator approximation when vibronic complexes are localized in the deepest potential well. There are arguments, however, to eliminate the second interpretation and favor the Raman-type relaxation. As $\delta_{12} = 240\ \mathrm{cm}^{-1} \gg \Delta_1 = 117\ \mathrm{cm}^{-1}$, the phonon-controlled tunneling via the first excited vibronic state suggested by the value of the D_1 coefficient is not possible.

The second argument results from the phase relaxation studies, which give the Δ_1-value, as is described in the next section. Moreover, we have found in comparative relaxation studies of the Cu^{2+} and Mn^{2+} (non-Jahn–Teller ion) in Tutton salts having very similar adiabatic potential surface to that in Zn(L-aspartate) · $3H_2O$ that the Raman processes govern the relaxation for both ions with the same relaxation parameters (*5*). Thus, we conclude that the vibronic dynamics does not contribute significantly to the spin–lattice relaxation of the Cu^{2+} in Zn(L-aspartate) · $3H_2O$.

The existence of the linear aT-term in the interpretation of the experimental data needs some comments. This term does not describe the direct one-phonon relaxation process since its influence is observed up to 12 K (see Fig. 3), whereas the direct process can dominate below 4 K. Because instantaneous diffusion effects are observed, as will be discussed below, we can identify the linear term as due to the relaxation of Cu–Cu pairs (see Eq. [3]). The pairs can appear in the crystal as a result of a nonuniform distribution of the doped Cu^{2+} ions because of a relatively high Cu^{2+} concentration (higher than 10^{18} ion/cm^3).

IV. ELECTRON PHASE RELAXATION

1. Phase Relaxation Mechanisms: Decay of the ESE Amplitude

Dephasing of the precession motion of spins is observed as a decay $V(2\tau)$ of the electron spin-echo amplitude, which can be described by the exponential function

$$V(2\tau) = V_0 \exp(-m\tau^k), \qquad [7]$$

with $k = 0.5$–3, and the m-coefficient depends on the relaxation mechanism (*17*). The decay function in Eq. [7] can be described by a characteristic time T_{M}, called the phase memory time. For the single exponential function ($k = 1$) one can write $V(2\tau) = V_0 \exp(-2\tau/T_{\mathrm{M}})$, whereas for $k \neq 1$ we can define

$$T_{\mathrm{M}} = \left(\frac{1}{m}\right)^{1/k}. \qquad [8]$$

In pulsed EPR studies of paramagnetic ion complexes, because the pulse excitation band is much narrower than the EPR spectrum width, microwave pulses can excite only a part of the ions. In two-pulse EPR experiments, a second pulse refocuses the precession of the excited spins (spins A). Thus, only spins A contribute to the ESE signal amplitude; nonexcited spins B do not contribute, but can produce the dephasing of spins A. This dephasing (phase relaxation) may be a consequence of: (i) a decrease of the number of spins A, as a result of the electron spin diffusion converting spins A into spins B or/and spin–lattice relaxation processes; (ii) spectral diffusion and/or instantaneous diffusion due to random fluctuations of the phase of the precession produced by fluctuating local magnetic field. The total decay function is the product of the independent relaxation processes,

$$V(2\tau) = V_{\mathrm{SD}} \cdot V_{\mathrm{ID}} \cdot V_0, \qquad [9]$$

where the first two processes depend on the unpaired electron concentration and describe the effect of spectral diffusion within an electron spin system (V_{SD}) and the effect of the instantaneous diffusion (V_{ID}) produced by the refocusing pulse. The

last factor, V_0, considers concentration-independent contributions, dominating when interactions between unpaired electrons are negligible and

$$V_0 = V_{\mathrm{NSD}} \cdot V_{\mathrm{motion}} \cdot V_{\mathrm{spin-lattice}}. \quad [10]$$

When the effects of V_{SD} and V_{ID} are negligible, the role of spins B is played by the nuclear spins, and the phase relaxation at rigid lattice limit is governed by nuclear spectral diffusion,

$$V_{\mathrm{NSD}} = V_0 \exp(-m\tau^k), \quad [11]$$

where (*18*)

$$m = 2\pi W_{\mathrm{n}} c_{\mathrm{n}} \left(\frac{\mu_0}{4\pi} 3 r_{\mathrm{n}} \gamma_{\mathrm{n}} \gamma_{\mathrm{e}} \hbar\right)^{3/4}.$$

In Eq. [11], W_{n} is the nuclear flip–flop rate due to internuclear dipolar coupling, c_{n} is the concentration of the nuclei, and r_{n} is an average internuclear distance. The theory predicts that the index k depends on the interpulse distance τ : $k = 7/4$ for long τ and $k = 3$ for short τ. In practice $k = 2$ is observed (*17, 18*). The phase memory rate $1/T_{\mathrm{M}}$ due to the nuclear spectral diffusion is temperature independent and is determined by distribution of the magnetic nuclei in the crystal. This gives the rigid lattice limit value T_{M} that, as a rule, is longer than 0.1 μs for proton NSD in molecular crystals and can be influenced by molecular motion (V_{motion}) and by spin–lattice relaxation processes ($V_{\mathrm{spin-lattice}}$) at higher temperatures (*16*).

2. Experimental T_{M} Values and Temperature Variations

The observed decay of the ESE amplitude for Cu^{2+} in Zn(L-aspartate)$\cdot 3H_2O$ (shown for $T = 10$ K in Fig. 4) is single exponential $V(2\tau) = V_0 \exp(-2\tau/T_{\mathrm{M}})$ in the whole temperature range. The temperature variation of the phase relaxation rate $1/T_{\mathrm{M}}$ is shown in Fig. 5.

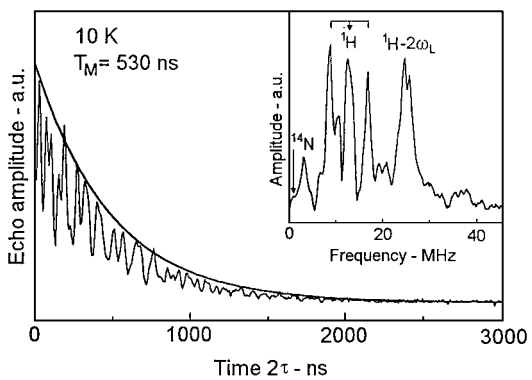

FIG. 4. Electron spin echo (ESE) decay at 10 K. The best fit, obtained with a single exponential function with $T_{\mathrm{M}} = 0.53$ μs, is shown as the solid line. The Fourier transform of the modulation function is shown in the inset. The peaks assigned to ^{14}N, ^{1}H, and ^{1}H-overtones are marked.

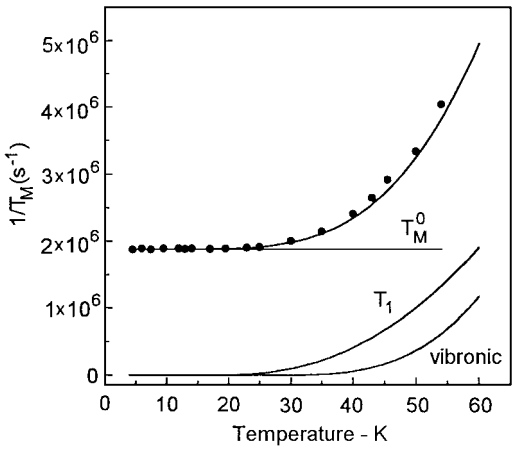

FIG. 5. Temperature dependence of the phase relaxation rate $1/T_{\mathrm{M}}$. The solid line through the experimental points is the best fit calculated with Eq. [14]. The three contributions to the total rate are shown separately as T_{M}^0, rigid lattice value; T_1, spin–lattice relaxation contribution, and vibronic phonon-controlled tunneling through vibronic level of energy $\Delta = 243$ cm^{-1}.

2.1. Rigid Lattice Dephasing Rate

Below 20 K the dephasing rate is temperature independent with $1/T_{\mathrm{M}}^0 = 1.88$ MHz and the decay function of the $\exp(-b\tau)$-type. For nuclear spectral diffusion of protons the decay function of $\exp(-b\tau^2)$-type is expected and the dephasing rate due to this mechanism can be evaluated from Eq. [11] taking $c_{\mathrm{n}} = 5.2 \times 10^{28}$ m^{-3} (for 44 protons in the unit cell with volume 841.97×10^{-30} m^3 (*24*)), and proton–proton flip–flop rate (*18*)

$$W_{\mathrm{n}} = \left(\frac{\mu_0}{4\pi}\right) \frac{\gamma_{\mathrm{n}}^2 \hbar}{10} c_{\mathrm{n}} = 3925\,\mathrm{s}^{-1}. \quad [12]$$

For $k = 2$, Eq. [11] gives a dephasing rate $1/T_{\mathrm{M}}^0(\mathrm{NSD}) = 0.14$ MHz. Thus, the NSD gives a negligible contribution to the total rate. Another temperature-independent contribution can be expected from the electron spectral diffusion and instantaneous diffusion.

Spectral diffusion (SD) arises from dipolar coupling between nonexcited spins B which produce dephasing of the excited spins A. A random distribution or spins B results in a distribution of the dipolar flip–flop rates, but the SD effects depend mainly on the most probable rate which can be calculated as (*17, 43*),

$$W_{\max} = \left(\frac{\mu_0}{4\pi}\right)^2 \frac{2^5\pi^3}{3^6} \gamma_{\mathrm{e}}^4 \hbar^2 c_{\mathrm{B}}^2 \frac{\Delta\omega_{1/2}}{\Delta\omega_k^2} \left(\ln \frac{\Delta\omega_{\mathrm{k}}}{2\Delta\omega_{1/2}}\right)^2, \quad [13]$$

where $c_{\mathrm{B}}[\mathrm{m}^{-3}]$ is the concentration of the spins B. The $\Delta\omega_{\mathrm{i}}$ is the half-width at half-height. The $\Delta\omega_{\mathrm{k}}$ is the experimental linewidth, due to the unresolved spin packets, equal to $\Delta\omega_{\mathrm{k}} = 23$ G $= 43.8$ MHz, and the dipolar linewidth $\Delta\omega_{1/2}$ can be calculated as $\Delta\omega_{1/2} = (\mu_0/4\pi)3.8\gamma_{\mathrm{e}}^2 \hbar\, c_{\mathrm{e}} = 17.4$ MHz. Thus, the

most probable flip–flop rate is equal to $W_{max} = 1.1 \times 10^5$ s^{-1}, indicating that the SD is in the fast range for which the ESE decay rate is $1/T_M^0(\mathrm{SD}) = 2.5 \times 10^{-19} c_B = 1.65$ MHz. This is very close to the observed value of 1.88 MHz.

Instantaneous diffusion (ID) is due to the second pulse acting on spins A only. This refocusing pulse reverses spins A and produces perturbation of the dipolar coupling between on-resonance spins which is a source of the spin-precession phase randomization (*18*). The resulting decay of the ESE is described by the function $V(2\tau) = V_0 \exp(-2b\tau)$ with $b = \Delta\omega_{1/2} \sin^2(\Theta/2) c_A/c_e$, where Θ is the magnetization turning angle which is equal to $2\pi/3$ for Hahn-type ESE. Thus, the phase relaxation rate due to the ID is equal to $1/T_M^0(\mathrm{ID}) = b = 0.82$ MHz.

The contributions from SD and ID have the same order of magnitude and the effective decay rate $1/T_M^0(\mathrm{SD} + \mathrm{ID}) = 2.47$ MHz is slightly larger than the experimental value 1.88 MHz. This is, however, a relatively good approximation in light of the experimental error in Cu^{2+} concentration determination and an estimation of the dipolar linewidth $\Delta\omega_{1/2}$.

2.2. Temperature Dependence of the Dephasing Rate

The dephasing rate can be influenced by temperature as a result of motions of the spin system. The motions can be the spin flips due to the spin–lattice relaxation processes as well as molecular vibrations of a paramagnetic center or surrounding matrix molecules. These motions can be related to vibronic dynamics, exchange-type jumps, fast spectral diffusion under dynamical EPR line narrowing, and vibrations of the centers with anisotropic EPR parameters. As these mechanisms are not well explained theoretically, we will describe the temperature dependence in terms of the spin packet model.

Spin packet model. Since $\Delta B_{packet} \propto 1/T_M$, an influence of molecular motions on T_M can be understood in terms of variations of the width of the spin packets giving rise to the inhomogeneously broadened EPR line (see Fig. 6a). This width can be determined from the Fourier transform of the decay function $V(2\tau)$.

Thermal motions of a paramagnetic complex or radical molecule having anisotropic g-tensor and/or hyperfine splitting A produce time-dependent shifts $\Delta g(t)$ and $\Delta A(t)$. The frequencies of these motions are about 10^{12}–10^{14} s^{-1} and produce

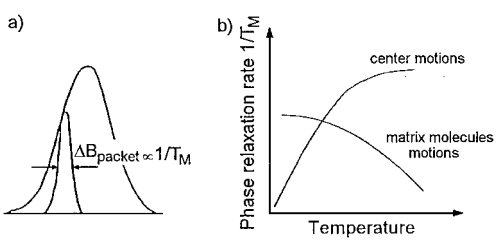

FIG. 6. (a) Single spin packet with width ΔB_{packet} under an EPR line influenced by molecular motions; (b) Temperature variations of the phase relaxation rate $1/T_M$ due to a paramagnetic center and matrix molecular motions.

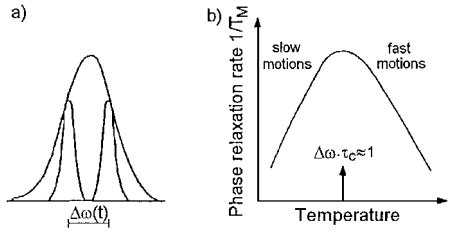

FIG. 7. (a) Two spin packets resulting from dipolar interaction in a two-spin system with splitting $\Delta\omega$ influenced by exchange-type dynamics; (b) Resonance enhancement of the phase relaxation rate $1/T_M$ as a result of a transition from slow to fast exchange limit.

homogeneous broadening of the individual spin packets, determining its linewidth ΔB_{packet}. Thus, an increase with temperature in the amplitude of the molecular motion should produce a continuous spin packet broadening, which is observed as an acceleration of the phase relaxation rate $1/T_M$ (Fig. 6b).

For slow molecular motions or high concentration of magnetic nuclei, the spin packet width can be determined by the local magnetic field fluctuations. In such a case, the motions of the matrix molecules can produce an averaging of the local field leading to spin packet narrowing upon heating. As the result, a continuous decrease in the phase relaxation rate can be expected (Fig. 6b).

Another resonance-type contribution of the molecular motion appears when spin packets are due to nonresolved superhyperfine structure from dipole–dipole coupled groups of nuclei like H_2O or NH_3 groups. In the case of a two-spin group, two spin packets splitted by $\Delta\omega$ are expected, as shown in Fig. 7a. If there exists an exchange-type process or jumps between states of the system characterized by the correlation time τ_c (like reorientations of molecular groups), then the two spin packets could merge. For slow transition rate ($1/\tau_c \ll \Delta\omega$), two separated spin packets are hidden under the EPR line. When the transition rate increases, the packets broaden, and for $1/\tau_c \approx \Delta\omega$ the packets merge into a single broad line. This line continuously narrows when $1/\tau_c$ increases. Such a transition from the slow to the fast motion limit can be observed when the transitions are thermally activated. It produces a maximum in the temperature dependence of $1/T_M$ (Fig. 7b), as was observed for rotating CH_3 groups in nitroxide molecules (*44*) and NH_3 groups in crystals (*45–47*).

The increase in $1/T_M$ for Zn(L-aspartate) · $3H_2O$:Cu^{2+} (see Fig. 5) has no resonant character and is due to the Cu complex motions. The motions can be identified as excitations to the higher energy level and as the spin–lattice relaxation flips of the spins. They are described by the second and third terms in the following equation, which fit well the experimental data,

$$\frac{1}{T_M} = \frac{1}{T_M^0} + w \exp\left(-\frac{\Delta}{kT}\right) + \alpha \frac{1}{T_1}, \qquad [14]$$

where $1/T_M^0 = 1.88 \times 10^6\ s^{-1}$ is the rigid lattice limit dephasing rate discussed in Section IV.2.1. The fitting parameters are $w = 4.0 \times 10^8\ s^{-1}$, $\Delta = 243\ cm^{-1} = 174\ K$, $\alpha = 0.5$, and T_1 is given by the Raman and linear contributions as described in Section III.2. The best fit is shown by the solid line in Fig. 5, where the three contributions are separately shown.

The exponential term describes thermal excitations to the first excited vibronic level of energy Δ. The coefficient w indicates that this dephasing mechanism can be understood as a phonon-controlled tunneling between two potential wells with tunneling frequency $w = 400$ MHz (see Fig. 8). The dephasing of the precessional spin motion due to this mechanism has not been considered theoretically in detail, but it was suggested (*48*) and observed by us for Cu^{2+} ions in different crystals (*5, 20, 39*). The possible excitations and relaxation back within the same potential well (Orbach–Aminov-type process) do not operate, since then w should be on the order of the vibrational frequency $10^{13}\ s^{-1}$. The contribution from spin–lattice relaxation processes is possible since there is a rapid increase in the $1/T_1$ relaxation rate, which becomes comparable to the dephasing rate above 40 K (Fig. 9). In that case the effective relaxation rate can be expected to be $1/T_2^* = 1/T_M + 1/(2T_1) = 1.5/T_1$ when $T_1 < T_M$. In our fitting $\alpha = 0.5$ in Eq. [14], indicating that the dephasing rate is not overdominated by spin–lattice relaxation processes.

Motional effects in the ESEEM spectrum. The width of the spin packet can be calculated as $\Delta B_{packet}[G] = 0.131 \times 10^{-6}/(g \cdot T_M[s])$. In the system studied here, for $g_z = 2.313$ (*24*), the width of the spin packet is 0.107 G at 4.2 K and increases to 0.227 G at 53 K as a result of the Cu complex motions. This broadening can be observed in the ESEEM spectra

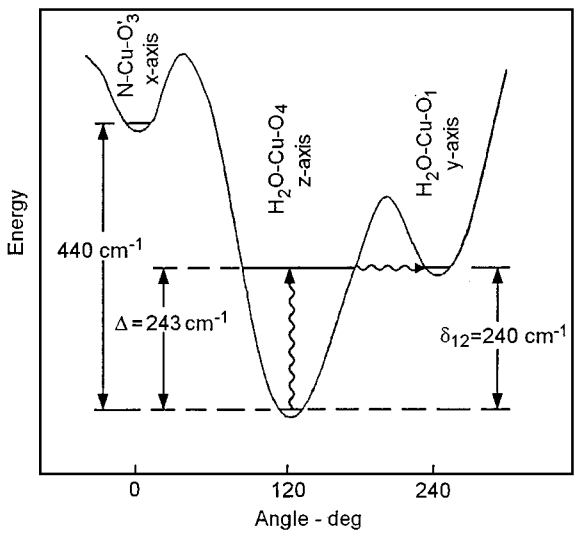

FIG. 8. Circular-cross section through the potential energy surface of the vibronic Zn(L-aspartate) · $3H_2O$:Cu^{2+} complex with vibronic levels determined from EPR and ESE measurements. The wavy lines show the phonon-controlled tunneling process between the wells.

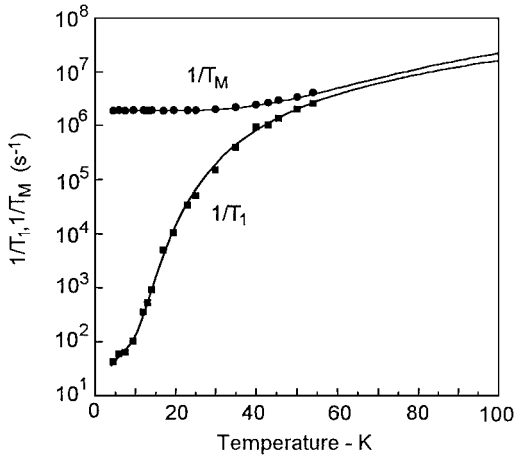

FIG. 9. Comparison of the temperature variations of the spin–lattice relaxation and the dephasing rate in the Zn(L-aspartate) · $3H_2O$:Cu^{2+}.

obtained as the Fourier transform of the function describing the modulation of the ESE amplitude. The modulated ESE decay at 10 K is shown in Fig. 4, where the inset presents the FT-ESE (ESEEM) spectrum. This pseudo-ENDOR-type spectrum consists of many lines from ^1H nuclei at the Larmor frequency ω_L with overtones at $2\omega_L$, as well as the peak from ^{14}N. At least one doublet around the matrix proton frequency (marked by arrow) is well seen in the proton lines region. This is due to the interactions with protons of the nearest water molecules. Resonances in the ESEEM spectrum are continuously broadened when the temperature increases, and the hyperfine structure is smeared out at about 50 K. The structures resolved in the ESEEM spectrum form unresolved spin packets of superhyperfine structure in the EPR spectrum of Zn(L-aspartate) · $3H_2O$:Cu^{2+}.

V. CONCLUSIONS

We have shown above that, although Cu^{2+} complexes in Zn(L-aspartate) · $3H_2O$ undergo the pseudo-Jahn–Teller effect, the electron spin–lattice relaxation is not governed by the vibronic dynamics below 50 K. The reason for this seems clear. There is a strong nonequivalence in energy among the three potential wells (distorted configurations of the octahedral Cu^{2+} complexes) formed by the Jahn–Teller effect in the adiabatic potential surface. Because of this nonequivalence, the coherent tunneling between the ground vibronic states of neighbor wells does not operate, and the complexes are localized in the deepest potential well at low temperatures. However, the dominant mechanism of the phase relaxation is related to the vibronic dynamics and occurs through the phonon-controlled excitations to the higher energy level of energy $\Delta = 243(5)\ cm^{-1}$. These data, together with our previously published cw-EPR results (*24*), allow one to draw the vibronic energy levels scheme in the wells of the adiabatic potential surface of the Cu complex in Zn(L-aspartate) · $3H_2O$, as shown in Fig. 8. Two vibronic levels are

localized in the deepest potential well, appearing along the z-axis of the Cu^{2+} complexes, with splitting Δ. The value of Δ is practically the same as the energy $\delta_{12} = 240\ cm^{-1}$ of the ground vibronic level in the second potential well which was determined from the temperature variations of the g-factor (*24*). Thus, the tunneling from the level Δ to the level δ_{12} and rapid back relaxation are an effective mechanism of the phase relaxation and the driving mechanism of Jahn–Teller dynamics.

Our results clearly show an advantage of the cw- and pulsed EPR methods in the determination of vibronic energy levels, which are not easy to determine by other spectroscopic techniques in the case of a low concentration of vibronic complexes in crystals.

REFERENCES

1. "Spin–Lattice Relaxation in Ionic Solids" (A. A. Manenkov and R. Orbach, Eds.), Harper & Row, New York, 1966. This book collects reprints of a very complete set of the major theoretical and experimental papers published on spin relaxation prior to 1965.
2. R. Orbach and H. J. Stapleton, *in* "Electron Paramagnetic Resonance" (S. Geschwind, Ed.), Ch. 2, Plenum, New York, 1972.
3. M. K. Bowman and L. Kevan, *in* "Time Domain Electron Spin Resonance" (L. Kevan and R. N. Schwartz, Eds.), Ch. 3, Wiley, New York, 1979.
4. Y. Zhou, B. E. Bowler, G. R. Eaton, and S. S. Eaton, Electron spin–lattice relaxation rates for $S = 1/2$ molecular species in glassy matrices or magnetically dilute solids at temperatures between 10 and 300 K, *J. Magn. Reson.* **139,** 165–174 (1999).
5. S. K. Hoffmann, M. A. Augustyniak, J. Goslar, and W. Hilczer, Does the Jahn–Teller effect influence electron spin relaxation? Electron paramagnetic resonance and electron spin echo studies of the Mn^{2+} doped $(NH_4)_2Mg(SO_4)_2 \cdot 6H_2O$ single crystal and comparison with Cu^{2+} data, *Mol. Phys.* **95,** 1265–1273 (1998).
6. M. K. Bowman, *in* "Magnetic Resonance of Carbonaceous Solids" (R. E. Botto and Y. Sanada, Eds.), Ch. 5, Am. Chem. Soc., Washington, 1993.
7. T. R. Askew, P. J. Muench, H. J. Stapleton, and K. L. Brower, Electron paramagnetic resonance and relaxation of amorphous silicon below 1K, *Sol. State Commun.* **49,** 667–670 (1984).
8. P. Raghunathan, Evidence for fractal dimension in asphaltene polymers from electron-spin-relaxation measurements, *Chem. Phys. Lett.* **182,** 331–335 (1991).
9. S. B. Stevens and H. J. Stapleton, Electron-spin-relaxation in Yb^{3+}-doped silicate glass, *Phys. Rev. B* **42,** 9794–9801 (1990).
10. W. M. Rogers and R. L. Powell, "Tables of Transport Integrals," Natl. Bar.Stand. (U.S.), Circ. (1958).
11. S. K. Hoffmann, W. Hilczer, and J. Goslar, EPR, electron spin–lattice relaxation, and Debye temperature of Cu(II)-doped triglycine selenate crystal, *J. Magn. Reson. A* **122,** 37–41 (1996).
12. J. A. Sussmann, Quantum mechanical theory of barrier crossing by ions in solids *J. Phys. Chem. Sol.* **28,** 1643–1648 (1967).
13. F. S. Ham, *in* "Electron Paramagnetic Resonance" (S. Geshwind, Ed.), Ch. 1, Plenum, New York, 1972.
14. S. K. Misra, Spin–lattice relaxation time in amorphous materials as affected by exchange interaction, tunneling level states (TLS) centres and fractons, *Spectr. Acta A* **54,** 2257–2267 (1998).
15. L. R. Dalton, A. L. Kwiram, and J. A Cowen, Electron spin–lattice relaxation in molecular crystals: $S = 1/2$, *Chem. Phys. Lett.* **17,** 495–499 (1972).
16. W. Hilczer, S. K. Hoffmann, J. Goslar, J. Tritt-Goc, and M. Augustyniak, Electron spin echo studies of spin–lattice and spin–spin relaxation of SeO_3^- radicals in $(NH_4)_3H(SeO_4)_2$ crystal, *Sol. State Commun.* **85,** 585–587 (1993).
17. K. M. Salikhov, A. G. Semenov, and Yu. D. Tsvetkov, "Electron Spin Echoes and Their Applications," Science, Novosibirsk, 1976.
18. K. M. Salikhov and Yu. D. Tsvetkov, *in* "Time Domain Electron Spin Resonance" (L. Kevan and R. N. Schwartz, Eds.), Ch. 7, Wiley, New York, 1979.
19. I. M. Brown, *in* "Time Domain Electron Spin Resonance" (L. Kevan and R. N. Schwartz, Eds.), Ch. 6, Wiley, New York, 1979.
20. S. K. Hoffmann, J. Goslar, W. Hilczer, M. A. Augustyniak, and M. Marciniak, Vibronic behavior and electron spin relaxation of Jahn–Teller complex $Cu(H_2O)_6^{2+}$ in $(NH_4)_2Mg(SO_4)_2 \cdot 6H_2O$ single crystal, *J. Phys. Chem. A* **102,** 1696–1707 (1998).
21. S. J. Lippard and J. M. Berg, "Principles of Bioinorganic Chemistry," University Science Books, Mill Valley, 1994.
22. R. Calvo, C. A. Steren, O. E. Piro, T. Rojo, F. J. Zuniga, and E. E. Castellano, Crystal structure and magnetic properties of diaqua(L-aspartate)copper(II), *Inorg. Chem.* **32,** 6016–6022 (1993).
23. R. Calvo, M. C. G. Passeggi, N. O. Moreno, G. E. Barberis, A. B. Chaves, B. C. M. Torres, L. Lezama, and T. Rojo, Magnetic properties of Cu(L-aspartato)$(H_2O)_2$: A linear chain antiferromagnet, *Phys. Rev. B* **60,** 1197–1203 (1999).
24. M. B. Massa, S. D. Dalosto, M. G. Ferreyra, G. Labadie, and R. Calvo, Vibronic behavior and single crystal EPR spectra of Cu(II) in copper doped diaqua(L-aspartato)zinc(II) hydrate, *J. Phys. Chem. A* **103,** 2606–2617 (1999).
25. B. L. Silver and D. Getz, ESR of $Cu^{2+}(H_2O)_6$. II. A quantitative study of the dynamic Jahn–Teller effect in copper doped zinc Tutton's salt, *J. Chem. Phys.* **61,** 638–650 (1974).
26. M. J. Riley, M. A. Hitchman, and A. W. Mohammed, Interpretation of the temperature dependent g-values of the $Cu(H_2O)_6^{2+}$ ion in several host lattices using a dynamic vibronic coupling model, *J. Chem. Phys.* **87,** 3766–3778 (1987).
27. M. A. Augustyniak and A. E. Usachev, The host lattice influence on the Jahn–Teller effect of the $Cu(H_2O)_6^{2+}$ complex studied by EPR in $K_2Zn(SO_4)_2 \cdot 6H_2O$ and $(NH_4)_2Zn(SO_4)_2 \cdot 6H_2O$ Tutton salt crystals, *J. Phys.: Condens. Matter* **11,** 4391–4400 (1999).
28. J. Murphy, Spin–lattice relaxation due to local vibrations with temperature-independent amplitudes, *Phys. Rev.* **145,** 241–247 (1966).
29. Y. Zhou, B. E. Bowler, G. R. Eaton, and S. S. Eaton, Electron spin–lattice relaxation rates for high-spin Fe(III) complexes in glassy solvents at temperatures between 6 and 298 K, *J. Magn. Reson.* **114,** 115–122 (2000).
30. Ch. Y. Huang, Optical phonons in electron spin relaxation, *Phys. Rev.* **154,** 215–219 (1967).
31. K. J. Standley and R. A. Vaughan, "Electron Spin Relaxation Phenomena in Solids," Hilger, London, 1969.
32. M. H. Rakowsky, K. M. More, A. V. Kulikov, G. R. Eaton, and S. S. Eaton, Time-domain electron paramagnetic resonance as a probe of electron–electron spin–spin interaction in spin-labeled low-spin iron porphyrins, *J. Am. Chem. Soc.* **117,** 2049–2057 (1995).
33. M. K. Bowman and L. Kevan, An electron spin–lattice relaxation mechanism involving tunneling modes for trapped radicals in glassy matrices. Theoretical development and application to trapped electrons in γ-irradiated ethanol glasses, *J. Phys. Chem.* **81,** 456–461 (1977).
34. A. Deville, B. Gaillard, C. Blanchard, and J. Livage, Electron spin–lattice relaxation in a true amorphous material: V^{4+} in V_2O_5, *J. Phys.* **44,** 77–85 (1983).
35. T. R. Askew, H. J. Stapleton, and K. L. Brower, Anomalous electron-spin relaxation in amorphous silicon, *Phys. Rev. B* **33,** 4455–4463 (1986).

36. M. B. Schulz and C. D. Jeffries, Spin–lattice relaxation of rare-earth ions in LaF_3, *Phys. Rev.* **149,** 270–288 (1966).

37. J. Pescia, S. K. Misra, M. Zaripov, and Y. Servant, Spin–lattice relaxation in the polymer resin poly-4-vinylpyridine doped with transition ions Cu^{2+}, Cr^{3+}, Mn^{2+}, and Gd^{3+} possessing weak spin–orbit coupling, *Phys. Rev. B* **59,** 9442–9446 (1998).

38. F. I. B. Williams, D. C. Krupka, and D. P. Breen, Relaxation in a Jahn–Teller system. II, *Phys. Rev.* **179,** 255–272 (1969).

39. S. K. Hoffmann and V. A. Ulanov, Off-centre dynamic Jahn–Teller effect studied by electron spin relaxation of Cu^{2+} ions in SrF_2 crystals, *J. Phys.: Condens. Matter* **12,** 1855–1866 (2000).

40. I. M. Zaritskii, V. Ya Bratus, V. S. Vikhnin, A. S. Vishnevskii, A. A. Kothits, and V. M. Ustintsev, Spin–lattice relaxation of nitrogen Jahn–Teller center in diamond, *Fiz. Tverd. Tela* (Russian) **18,** 3226–3230 (1976).

41. V. S. Vikhnin, Orientational relaxation and spin–lattice relaxation via phonon tunneling controlled process, *Fiz. Tverd. Tela* (Russian) **20,** 1340–1346 (1978).

42. C. J. Terblanche and E. C. Reynhardt, Room-temperature field dependence of the electron spin–lattice relaxation times of paramagnetic P1 and P2 centers in diamond, *Chem. Phys. Lett.* **322,** 273–279 (2000).

43. A. D. Milov, K. M. Salikhov, and Yu. D. Tsvetkov, Effect of spin dipole–dipole interaction on phase relaxation in magnetic diluted solids, *J. Exp. Theor. Phys.* (Russian) **63,** 2329–2335 (1972).

44. Yu. D. Tsvetkov and S. A. Dzuba, Pulsed ESR and molecular motions, *Appl. Magn. Reson.* **1,** 179–194 (1990).

45. S. K. Hoffmann, W. Hilczer, and J. Goslar, Electron spin echo studies of flipping type minimum in phase memory time of Cu(II) ions in triglycine selenate crystal at low temperatures, *Solid State Commun.* **100,** 449–452 (1996).

46. M. Gramza, W. Hilczer, J. Goslar, and S. K. Hoffmann, Electron spin relaxation and ESEEM spectroscopy of the glycine radical in diglycine nitrate single crystal, *Acta Chim. Scand.* **51,** 556–561 (1997).

47. J. Goslar, W. Hilczer, and P. Morawski, Low temperature dynamics of hydrazinium ions in lithium hydrazinium sulphate (LHS) studied by electron spin echo (ESE) technique, *Solid State Ionics* **127,** 67–72 (2000).

48. H. Bill and R. A. Silsbee, Dynamic Jahn–Teller and reorientation effects in the EPR spectrum of CaF_2: O_2^-. *Phys. Rev. B* **10,** 2697–2709 (1974).